# Ab Initio Molecular Dynamics Shows Low-Frequency Mode Manifolds Mediate $CO + CO^+ \rightleftharpoons CO^+ + CO$ Electron Exchange[1]

**Sergei Skokov[†] and Ralph A. Wheeler***

*Department of Chemistry and Biochemistry, 620 Parrington Oval, Room 208, University of Oklahoma, Norman, Oklahoma 73019*

*Received: November 5, 1999; In Final Form: April 14, 2000*

Classical molecular dynamics with a Hartree−Fock potential (direct dynamics) was used for qualitative studies of energy and charge dynamics in the gas-phase $CO + CO^+ \rightleftharpoons CO^+ + CO$ electron exchange reaction. Three potential energy minima and two transition states with energies below the dissociation limit were found along the reaction path. The central global minimum corresponds to the $(CO)_2^+$ dimer previously observed in photoionization experiments and two local minima correspond to weakly bound $CO{\cdot\cdot}CO^+$ capture complexes. At 200 K the energy transfer rate constants for the capture complexes and the $(CO)_2^+$ dimer were found to be in the 0.6−15 $ps^{-1}$ range, large enough to ensure complete energy randomization on the isomerization time scale. Yet the energy transfer is strongly affected by the choice of the initial normal mode energies. Adiabatic modes and adiabatic mode manifolds were observed for several sets of MD trajectories. The coupling between nuclear motion and variation of atomic charges was studied by using Fourier transformation techniques. Fundamental new observations from this study include: (1) substantial transfer of partial charge occurs over a range of geometries, so electron transfer (ET) is not abrupt; (2) ET is mediated predominately by low-frequency bending modes of the $(CO)_2^+$ complex; and (3) CO stretching modes do not transfer energy to torsional or bending modes on the simulation time scale, so a basic tenet of transition state theory—energy randomization—should be tested experimentally.

## Introduction

Electron transfer (ET) is the basis for electrochemical and electronic devices, and plays a critical role in photosynthesis, respiration, and many enzymatic, inorganic, and organic reactions.[2−5] Understanding energy transfer is similarly important for understanding and controlling chemical reactions,[6,7] especially since assumptions of energy randomization inherent in transition state theories have been questioned.[8] Donor−acceptor complexes, excited-state charge transfer complexes, and ion pairs provide gas-phase "laboratories" where ET, energy transfer, and their interplay may be explored independently from complications of solvent.

The treatment of ET reactions is conveniently based on the Marcus model:[9] ET is considered thermally activated and its rate constant is given by transition state theory as

$$k_{ET} = A \exp\left(\frac{-\Delta G^{\neq}}{k_B T}\right)$$

where $k_B$ is the Boltzmann constant, $T$ is temperature, $\Delta G^{\neq}$ is the reaction's energy barrier, and $A$ depends on the barrier crossing frequency. For nonadiabatic and weakly adiabatic ET, Marcus related the barrier height to reaction exothermicity, $\Delta G°$, by the expression

$$\Delta G^{\neq} = \frac{(\Delta G° + \lambda)^2}{4\lambda}$$

where $\lambda$ is called the "reorganization energy" or the "intrinsic barrier" (the activation energy when $\Delta G° = 0$).[2−5] The reorganization energy is separated into a sum of intramolecular ($\lambda_i$) and solvent ($\lambda_s$) contributions, $\lambda = \lambda_i + \lambda_s$, and $\lambda_i$ is commonly estimated from reactant and product vibrational frequencies and geometrical differences.[2,3] A single, high-frequency mode is often assumed to couple most strongly with the reaction coordinate.[10] The theory expressed by eqs 1−2 has been modified to accommodate strongly adiabatic reactions and to interpolate between the adiabatic and nonadiabatic regimes.[2,3] Calculations have been designed to simulate intramolecular energy transfer[11] and intermolecular ET. To gain insight into the details of ET, for example, empirical or semiempirical quantum molecular dynamics (MD) simulations have been performed to evaluate $\lambda_s$ and the shape of the solvent-induced energy profile,[12] and quantum mechanical models have been constructed to calculate the effects of solvent polarization on $\lambda_s$.[12−14] The electronic couplings between electron donors and acceptors entering the prefactor $A$ in eq 1, as well as their distance dependence, have also been evaluated experimentally and computationally.[2−5,15,16] Most published molecular orbital (MO) calculations of electron donor−acceptor couplings use optimized geometries of precursor complexes assumed appropriate for ET,[16,17] whereas MD studies used as a reaction coordinate the extent of charge transfer or the energy gap between reactant and product surfaces.[13,14] In contrast, the present contribution shows how analysis of a geometrical reaction coordinate can also give useful, complementary information.

Of course, the reliability of previous treatments requires that the underlying assumption of Marcus theory, weak interaction of electron donors and acceptors along the reaction path, should be met. For ion−molecule reactions, electrostatic interaction typically leads to the formation of precursor complexes (capture complexes) before the transition state is reached. Modifications of Marcus theory have been proposed to account for the

[†] Current address: Department of Chemistry, Emory University, 1515 Pierce Dr., Atlanta, GA 30322.

* To whom correspondence should be addressed.

10.1021/jp993909g CCC: $19.00 
Published on Web 06/14/2000

formation of capture complexes, and thus to account for the electrostatic part of the interaction on the reaction pathway.[18−20] This modification reinstitutes the usefulness of the Marcus approach for reactions proceeding via the double-minimum potential well and the modification has been successfully applied to interpret the kinetics of slow ion−molecule reactions.[21] As the interaction becomes stronger the barrier for electron transfer completely vanishes. This situation is usually encountered in gas-phase reactions between diatomic molecules and ions proceeding with nearly collisional rates.[22] Such systems presumably can be described by single-minimum energy surfaces. Indeed, kinetic and spectroscopic studies indicate the formation of stable complexes between diatomics and their cations—for instance, $(NO)_2^+$, $(CO)_2^+$, and $(N_2)_2^+$—rather than transition states.[23−25]

The kinetics for both double-minimum and single-minimum systems is now well rationalized in the framework of Rice, Ramsperger, Kassel, and Marcus (RRKM)[26,27] and average dipole orientation (ADO)[22] theories, however, recent trajectory calculations[28] question the validity of the rapid energy randomization assumption for weakly bound ion−molecule complexes. Another intriguing problem involves microscopic charge dynamics. Marcus theory relates charge transfer with vibrational modes of noninteracting or weakly interacting species. If a capture complex is formed, questions naturally arise regarding the relations between charge transfer and the complex's degrees of freedom.

The present study describes the dynamics of charge and energy transfer in reactions of CO with its cation by using ab initio MD techniques. A discussion of recent experimental and theoretical studies addressing intramolecular energy transfer can be found in the article by Pan and Raff.[29] It is pertinent to note that previously reported theoretical studies of energy transfer were based on empirical potentials (though usually fitted to ab initio data). The choice of an ab initio potential in the present study was dictated by our interest in both energy and charge dynamics; the latter cannot be investigated by implementing empirical potentials. The present study also complements previous computational studies of ET by providing geometrical, energetic, and dynamical data for the $CO + CO^+ \rightleftharpoons CO^+ + CO$ reaction at unprecedented levels of detail.

**Computational Methods.** For the entire study, an MO/MD computer program similar to one described by Carmer et al.[30,31] was employed, but modified to use atomic forces from the ab initio MO computer program GAMESS.[32] In this MO/MD method, nuclear dynamics is governed by Newton's classical equations of motion. At each time step the system is treated as an instantaneous configuration of atomic nuclei and atomic forces are computed by ab initio methods within the Born−Oppenheimer approximation. The unrestricted Hartree−Fock (UHF) method with split valence plus polarization 6-31G(d) basis set was used for all MD simulations reported here. The algorithm proposed by Berendsen et al.[33] was implemented for temperature control. To generate dynamics trajectories, MD simulations were carried out for total (vibrational) energies ranging from 1 to 5 kcal/mol and a 0.5 fs time step, approximately an order of magnitude smaller than the time scale of any vibration. Energies in this range were chosen for computational speed and to ensure that energies in each vibrational mode, after equilibration, are near thermal energies. To generate the minimum energy path (MEP) for the electron exchange reaction, trajectories were quenched by setting all atomic velocities to zero immediately after the atoms pass through the energy maximum. All simulations other than those used to generate the MEP correspond to real-time dynamics simulations.

Although the results reported in the next section indicate the potential of ab initio MO/MD methods for studying ET, readers should be cognizant of several inherent limitations of the methods. First, even high-level ab initio quantum chemical methods are known to include some error in stationary point geometries and energies. Second, a potentially serious approximation in the quantum chemical methods used here involves neglecting electronic excited state mixing with the ground state. To test the severity of this approximation, we performed CISD/6-31G(d) calculations at large $CO\cdots CO^+$ separations and both CISD/6-31G(d) geometry optimizations and CASSCF(7,8)/aug-cc-pVDZ//UHF/6-31G(d) single-point calculations at stationary points on the energy surface, where ground and excited state mixing is likely to be most extensive. We found that at large $CO\cdots CO^+$ separations, the first excited state, $^2\Pi$, is 2.5 eV above the $^2\Sigma$ ground state, at the CISD/6-31G(d) level of theory. Moreover, the lowest energy excited state appears more than 2 eV above the ground state at both the CISD/6-31G(d) and CASSCF(7,8)/aug-cc-pVDZ//UHF/6-31G(d) levels for the transition states, intermediates, and precursor (successor) complexes on the reaction's energy surface. Thus, electronic excited states perturb the ground state very little and may be safely neglected in qualitative MO calculations. The large energy gap (2.5 eV) between the ground and lowest excited state energy surfaces likewise implies that the ET reaction is electronically adiabatic. Consequently, dynamics on electronic excited-state surfaces and transitions between energy surfaces may be neglected at the thermal energies ($E = 5$ kcal/mol) considered here. Finally, charges were determined by using Mulliken population analysis[34] and should therefore be interpreted to indicate only approximate *changes* in charge between different structures. Because configuration interaction (CI) methods with single excitations, rather than Hartree−Fock methods, are required to give the dipole moment of CO in the correct direction, qualitative geometries and charge distributions of all stationary points in the reaction were also verified by comparing HF/6-31G(d) and CISD/6-31G(d) calculations.

Vibrational spectra were computed from the results of MO/MD simulations by summing over all atoms the square of the Fourier transform of the Cartesian components of atomic velocities, according to the following equation:[35]

$$E(\omega) = \frac{1}{2}\sum_{j=1}^{n} m_j \sum_{\zeta=x,y,z} \frac{2}{L}\left|\int_0^L v_{j\zeta}(t) e^{i\omega t} \mathrm{d}t\right|^2$$

where $E(\omega)$ is the energy of the vibration with frequency $\omega$, $n$ is the number of atoms, $m_j$ is the mass of atom $j$, $L$ is the total time of the simulation, and $v_{j\zeta}$ is a Cartesian component of the velocity of atom $j$ at time $t$. Although it is customary to scale vibrational frequencies obtained from ab initio MO calculations to obtain better agreement with experiment,[36] no scaling was employed here. Because the curvature of the energy surface on which dynamics trajectories were propagated should reflect similar errors as calculated force constants used in more conventional MO calculations of vibrational frequencies, we focus the interpretation of our results on the close correlation between atomic and charge dynamics. Charge dynamics were analyzed by Fourier transforming the time-dependent charge on atom $j$, $q_j(t)$:

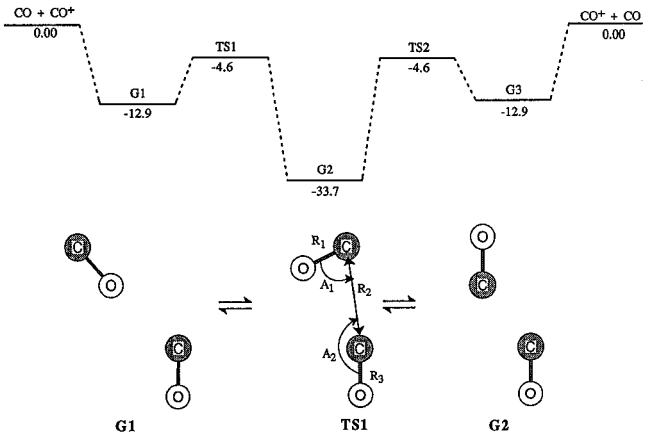


**Figure 1.** Top panel: Energy diagram for reaction 1 at the UHF/6-31G(d) level of theory. Numbers are the relative energies in kcal/mol. Bottom panel: Structure of the $CO\cdots CO^+$ capture complex, transition state, and $(CO)_2^+$ dimer.

**TABLE 1: Relative Energies and Mulliken Atomic Charges from UHF/6-31G(d) Calculations for Species Appearing in the Electron Exchange Reaction $CO + CO^+ \rightarrow CO^+ + CO$; G1, G2, and TS1 Are Sketched in Figure 1**

| species | relative $E$ (kcal/mol) | atomic charges (a.u.) C(1) | O(1) | C(2) | O(2) |
|---|---|---|---|---|---|
| $CO + CO^+$ | 0.00 | +0.27 | −0.27 | +0.93 | +0.07 |
| precursor complex G1 | −12.9 | +0.48 | −0.36 | +0.89 | −0.01 |
| transition state TS1 | −4.6 | +0.45 | −0.15 | +0.76 | −0.06 |
| intermediate G2 | −33.7 | +0.60 | −0.10 | +0.60 | −0.10 |

[a] Charge transfer calculated using CISD/6-31G(d) optimized geometries are slightly larger than those below (e.g. q(CO) = +0.18 for the precursor complex G1).

$$I(\omega) = \frac{2}{L}\sum_{j=1}^{n}\left|\int_0^L q_j(t)e^{i\omega t}\right|$$

To assist the investigation of intramolecular energy transfer, atomic velocities were projected onto the normal modes at each time step as proposed by Raff and co-workers.[37]

## Results and Discussion

The electron self-exchange reaction

$$CO + CO^+ \rightleftharpoons CO^+ + CO \qquad (1)$$

was chosen for the present study. First, we note that calculated distances for the reactants show r($CO^+$) = 1.098 Å and r(CO) = 1.114 Å. Although it might appear unusual that the carbon−oxygen distance in $CO^+$ is shorter than in CO, calculated distances are qualitatively consistent with those determined experimentally: r($CO^+$) = 1.1150 Å and r(CO) = 1.1281 Å.[38] Figure 1 shows a qualitative energy diagram and geometries of minima and transition states. Stationary states and transition states were computed using the GAUSSIAN94 computer program[39] at the UHF/6-31G(d) level. Table 1 summarizes atomic charges for the reactants, potential energy minima, and transition states shown in Figure 1. The potential energy surface (PES) for reaction 1 exhibits three minima and two transition states along the MEP. G1 represents a capture complex (a "precursor complex" to ET) with a calculated energy 12.9 kcal/mol below the energy of the separated $CO/CO^+$ species. The complex has the oxygen of CO 3.19 Å from the carbon of $CO^+$. G2 is a $C_{2h}$ symmetry intermediate with a calculated energy of −33.7 kcal/mol relative to the separated

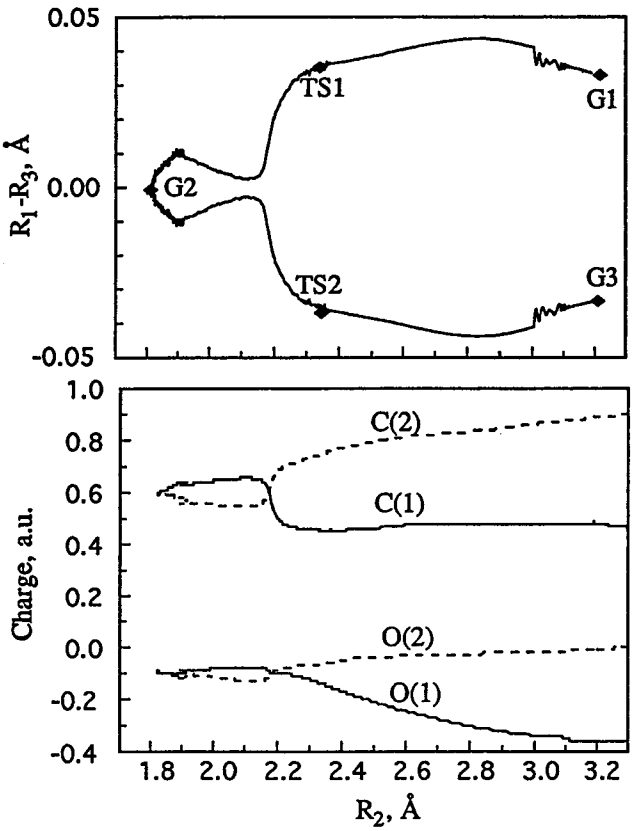


**Figure 2.** Top panel: Minimum energy path for reaction 1 computed from MO/MD simulations. Axis notation and notation for minima and transition states correspond to Figure 1. Bottom panel: Variation of atomic charges along the minimum energy path displayed in the top panel.

species and a relatively short C−C distance of 1.82 Å. An intermediate detected experimentally at 22−26 kcal/mol below the energy of $CO/CO^+$ indicates that calculated energies are qualitatively correct.[24] Finally, TS1 is the transition state between G1 and G2 and has a calculated CO oxygen to $CO^+$ carbon distance of 2.38 Å, with the carbon of CO tilted closer to the $CO^+$ fragment than in the G1 precursor complex. Atomic charges for each species indicated in Figure 1 are given in Table 1 and indicate that only 0.1 $e^-$ is transferred from CO to $CO^+$ in the precursor complex G1, whereas 0.3 $e^-$ is transferred before the structure reaches transition state TS1. An additional 0.2 $e^-$ is transferred from CO to $CO^+$ between TS1 and intermediate G2.

Figure 2a shows a two-dimensional projection of the MEP generated using (quenched) MO/MD simulations and Figure 2b shows the evolution of atomic charges along the MEP, as the carbon−carbon distance changes. The TS1 → G1 part of the trajectory was obtained from MD simulations started at the transition state by using a quenching technique and, to avoid "overshooting" near the transition state, the TS1 → G2 path was computed using the Berendsen temperature scaling algorithm[33] with temperature $T$ = 0.1 K. From G1 to TS1, the positive charge on CO increases almost monotonically as ET to $CO^+$ begins. An abrupt increase of positive charge on CO appears at C−C distances slightly shorter than the distance in TS1, followed by a very slight charge transfer upon moving to the intermediate G2. Such unexpected behavior deserves special comment. Clearly, the most abrupt ET on the entire reaction path occurs where the C−O bond distances also change most rapidly, in accord with Marcus theory, but after the transition state for $CO/CO^+$ association is already attained. In this range

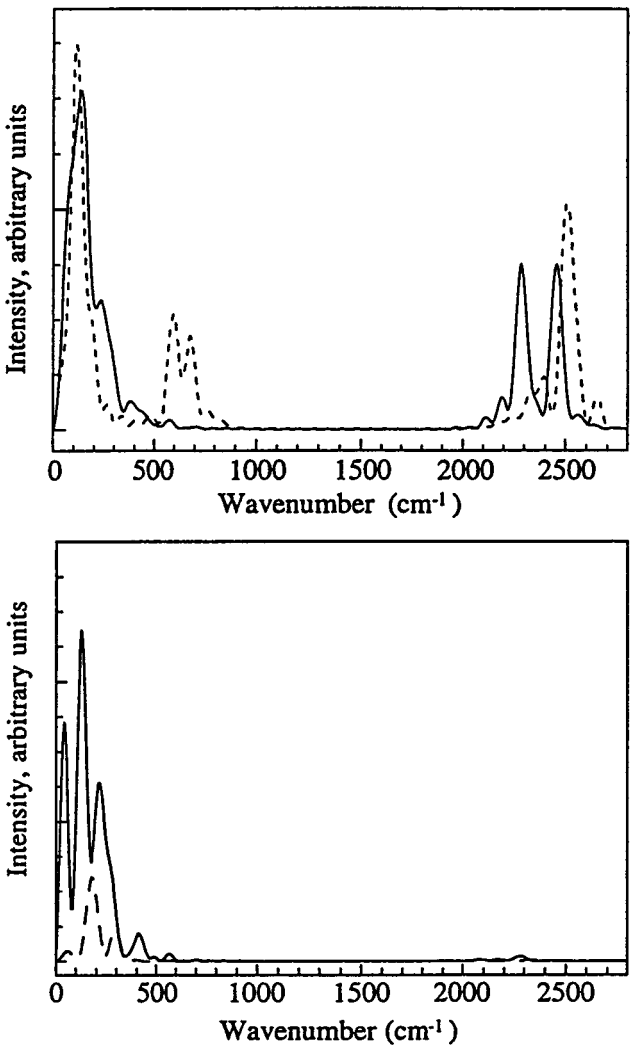


**Figure 3.** Top panel: Vibrational spectra for the precursor complex G1 (solid line) and the intermediate G2 (dashed line). Bottom panel: Charge oscillation spectra for G1 and G2 have significant intensities only at frequencies less than 600 $cm^{-1}$, corresponding to torsional and bending modes shown in the top panel. Only relative intensities within a single trace are meaningful. Data were determined from MO/MD simulations (unquenched) of 0.5 ps duration with initial kinetic energies of 1 kcal/mol in each mode.

of carbon−carbon distances (1.8−2.2 Å) the charges on CO fragments are opposite to those expected from their bond lengths: the longer carbon−oxygen bond corresponds to the larger positive charge. This, plus the pivoting of $CO^{\delta+}$ subunits required to bring the carbons of G1 and TS1 into close contact in G2, shows that motions other than bond length changes are dominant in mediating ET between CO and $CO^+$.

To determine which vibrational modes of $(CO)_2^+$ correlate most strongly with ET from CO to $CO^+$, we calculated vibrational spectra and charge oscillation spectra at the G1 and G2 geometries of $(CO)_2^+$. Figure 3 shows that charge oscillates between CO and $CO^+$ almost exclusively at frequencies below 600 $cm^{-1}$. The first column of Table 2 confirms that these low-frequency vibrational modes correspond to the bending and torsional modes of $(CO)_2^+$. Because spectral analyses at G1 and G2 do not necessarily reflect the reaction's evolution along the path shown in Figure 1, Table 2 also shows projected segments of the approximate reaction coordinate, and TS1's imaginary mode coordinate, on the normal coordinates of G1 and G2. First, mode 1 (associated with torsional rotation) is perpendicular to the MEP because all transition and ground state structures have

**TABLE 2: Projections of the Coordinate Corresponding to the Imaginary Mode of TS1 and the Approximate Reaction Coordinates from G1 to TS1 and from TS1 to G2 onto the Normal Coordinates of Precursor Complex G1 and Intermediate G2**

| frequency ($cm^{-1}$) and approximate description | projection of imaginary mode | projection of approximate reaction coordinate |
|---|---|---|
| G1 | TS1 | **Q**(TS1)−**Q**(G1) |
| 75, torsion rotation | 0.000 | 0.000 |
| 67, bending | 0.095 | 0.744 |
| 145, bending | 0.314 | 0.125 |
| 310, bending | −0.061 | 0.193 |
| 2266, CO stretch | 0.933 | 0.627 |
| 2452, $CO^+$ stretch | −0.132 | 0.013 |
| G2 | TS1 | **Q**(TS1)−**Q**(G2) |
| 133, torsion rotation, $A_u$ | 0.000 | 0.000 |
| 137, asym. bending, $B_u$ | 0.153 | −0.832 |
| 186, sym. bending, $A_g$ | 0.192 | 0.006 |
| 668, C−C stretch, $A_g$ | −0.395 | 0.185 |
| 2476, CO asym. stretch, $B_u$ | 0.673 | −0.219 |
| 2481, CO sym. stretch, $A_g$ | −0.576 | 0.475 |

The notation for stationary points is defined in Figure 1.

planar geometries. The largest component of the imaginary mode of TS1 in the G1 normal modes ansatz is the CO stretching mode (fifth mode), while overall motion along the TS1 → G1 path is mostly associated with bending (second mode). Similarly, the largest components of the imaginary mode of TS1 in the G2 normal coordinates ansatz are those associated with stretching vibrations, modes 5 and 6, while overall motion along TS1 → G2 is again associated with bending motion. In other words, the reaction path is curved, as can also be seen in Figure 2, and the implication of the path curvature will be discussed later. Here we simply note that Figure 3 and the last two columns of Table 2 indicate that C−O stretching is important near TS1, but $(CO)_2^+$ bending makes the dominant contribution to the reaction coordinate from G1 to TS1 and from TS1 to G2, where the majority of the ET occurs. Thus, estimation of reorganization energies should account for all vibrational modes, not just a small subset. Furthermore, the highest frequency modes are not always the modes that couple most strongly with ET. The correlation between charge oscillation and bending/torsional vibrations also implies that such dynamic charge polarization, frequently a missing component of reaction dynamics studies using empirical potentials (even those including static polarizability), is important. The general similarity of nuclear and charge dynamics demonstrated in Figure 3 offers the possibility for fitting atomic charges as a function of internal coordinates, in the same fashion as potential energy surfaces are parametrized for nuclear motion. From the comparison of relative intensities of charge spectra for the G1 and G2 complexes, one can see that dynamic charge polarization appears to be especially important for weakly bound complexes.

We now turn to the investigation of energy transfer dynamics. Energy transfer kinetics can be approximated by a simple exponential model[37]

$$\frac{dE_i}{dt} = \sum_{j=1}^{N} (k_{ji}E_j - k_{ij}E_i) \quad \text{and} \quad k_i = \sum_{j=1}^{N} k_{ij} \qquad (2)$$

where $E_i$ is the average total energy in mode $i$, $N$ is the number of modes, $k_{ij}$ values are the mode-to-mode energy transfer rate constants, and $k_i$ is the rate constant for energy transfer from the $i$-th mode. The first set of 12 MD simulations was carried out to evaluate energy transfer coefficients $k_i$ for each normal mode of G1 and G2 listed in Table 2. Energy transfer was

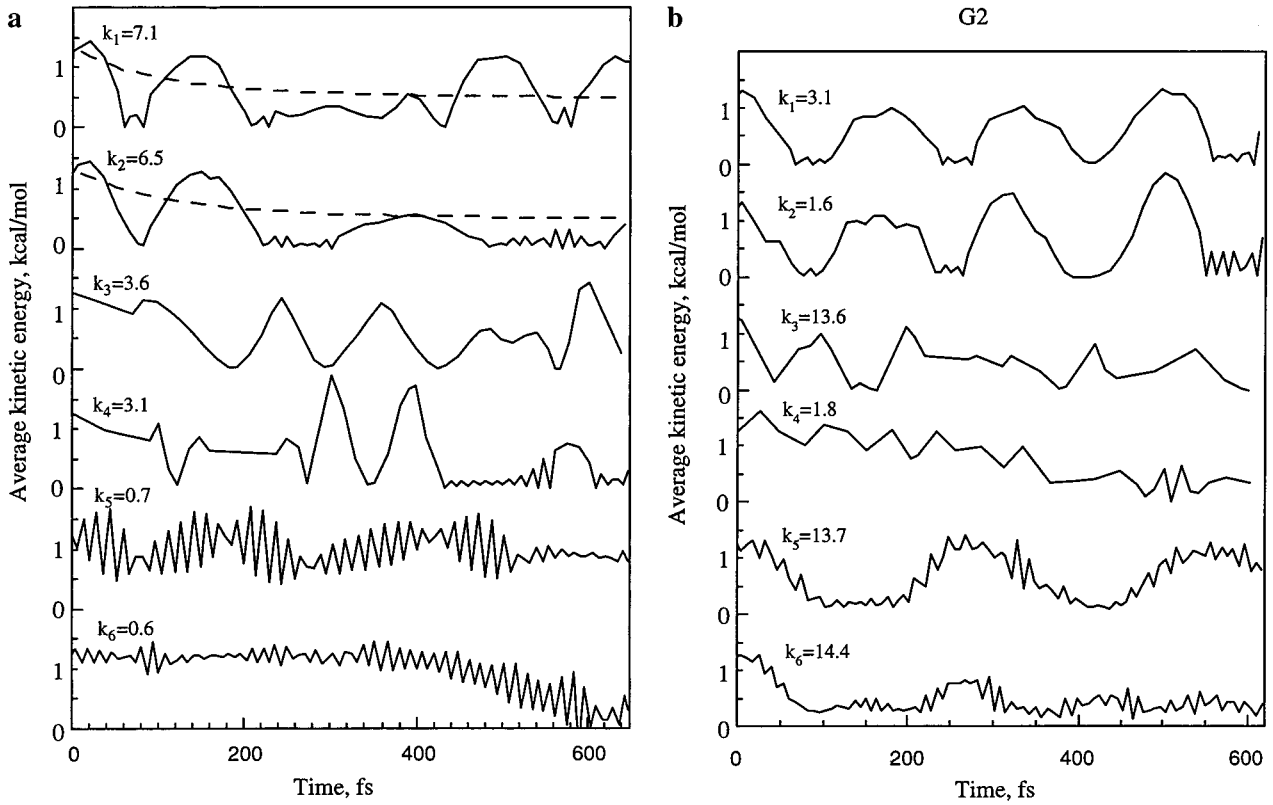


**Figure 4.** (a) Evolution of average normal mode kinetic energy in structure G1. The initial kinetic energy of the mode of interest was set to 2.5 kcal/mol and the energy of all other modes was set to 0.5 kcal/mol. Numbers are the rate constants (in $ps^{-1}$) for energy flow out of the mode of interest and dashed lines are representative curve fits. Each successive curve is displaced upward by 2 kcal/mol for clarity. (b) Evolution of average normal mode kinetic energy in structure G2. The initial kinetic energy of the mode of interest was set to 2.5 kcal/mol and the energy of all other modes was set to 0.5 kcal/mol. Numbers are the rate constants (in $ps^{-1}$) for energy flow out of the mode of interest. Each successive curve is displaced upward by 2 kcal/mol for clarity.

simulated by using a "pumping" technique, i.e., starting an MD trajectory from the G1 or G2 minimum energy geometry with initial kinetic energy of 2.5 kcal/mol in the mode of interest and 0.5 kcal/mol in each other mode. The time evolution of the average kinetic energy in the modes of interest is displayed in Figure 4. Because the vibrational periods for different normal modes are quite different, we averaged the energy in each mode over its own vibrational period. The coefficients $k_i$ were then evaluated by simultaneously fitting the 15 mode-to-mode coefficients in eq 2. In Figure 4 the exponential falloff can only be seen for a short initial period of time and is quickly washed out by fluctuations of energy among various modes. This prevents accurate fitting of energy transfer coefficients and thus our coefficients displayed in Figure 4 should be considered to be only crude estimates. For the G1 structure, energy transfer from the low-energy torsional and bending modes occurs on the time scale of 0.15−0.3 ps, while energy transfer from high energy stretching modes occurs on the time scale of 1.5 ps. In contrast, the stretching modes of G2 relax much faster than its low-energy modes, within 0.1 ps. In all MD simulations discussed above the average kinetic energy was 0.4 kcal/mol per mode, which corresponds to the equilibrium temperature of 200 K. At this temperature the G1 → G2 isomerization is much slower than the energy transfer rates. However, this does not guarantee the validity of statistical theories, which require fast energy randomization for any set of initial conditions (initial normal mode energies).

A second set of MD simulations was carried out to investigate the dynamics of mode-to-mode energy transfer processes, emphasizing three different types of normal modes: (1) the torsional rotation (mode 1), (2) bending vibrations (modes 2, 3, and 4), and (3) stretching vibrations (modes 5 and 6). First, two MD simulations were started from the ground-state G1 and G2 geometries with initial kinetic energies of 5 kcal/mol in the torsional modes. Figure 5 shows the time evolution of kinetic energy in normal modes during the MD simulation. For the G1 structure all modes become excited, whereas for the G2 structure modes 2 and 5 remained unexcited throughout 3 ps of simulation time. The latter results can be rationalized by noticing that the torsional rotation, mode 1, has $A_u$ symmetry, while antisymmetric bending mode 2 and antisymmetric stretching mode 5 both have $B_u$ symmetry (Table 2). Even though torsional rotation reduces symmetry from $C_{2h}$ to $C_2$, mode 1 still retains $A$ symmetry while modes 2 and 5 retain $B$ symmetry. In the next MD simulation we started from the G1 structure with zero initial kinetic energy in the torsional mode and 1 kcal/mol in each of the other modes. The results of this simulation, displayed in Figure 6, indicate no energy transfer from modes 2−5 to the torsional coordinate. At first glance this simulation, in connection with the previous simulation for the G1 structure (Figure 5a), appears to contradict the principle of microscopic reversibility because the mode-to-mode rate coefficients $k_{1i}$ are nonzero in one case (Figure 5a), whereas all $k_{i1}$ are essentially zero in the second case (Figure 6). The apparent contradiction is of course fictitious, since neither rate coefficient is properly averaged. The discrepancy, however, emphasizes the dependence of the mode-to-mode energy transfer rates on initial conditions. Zero $k_{i1}$ coefficients correspond to the specific set of conditions, namely, zero initial potential energy of the torsional mode, whereas nonzero $k_{1i}$ coefficients correspond to randomized torsional motion. The effect of initial conditions upon the energy transfer rates is usually quickly washed out

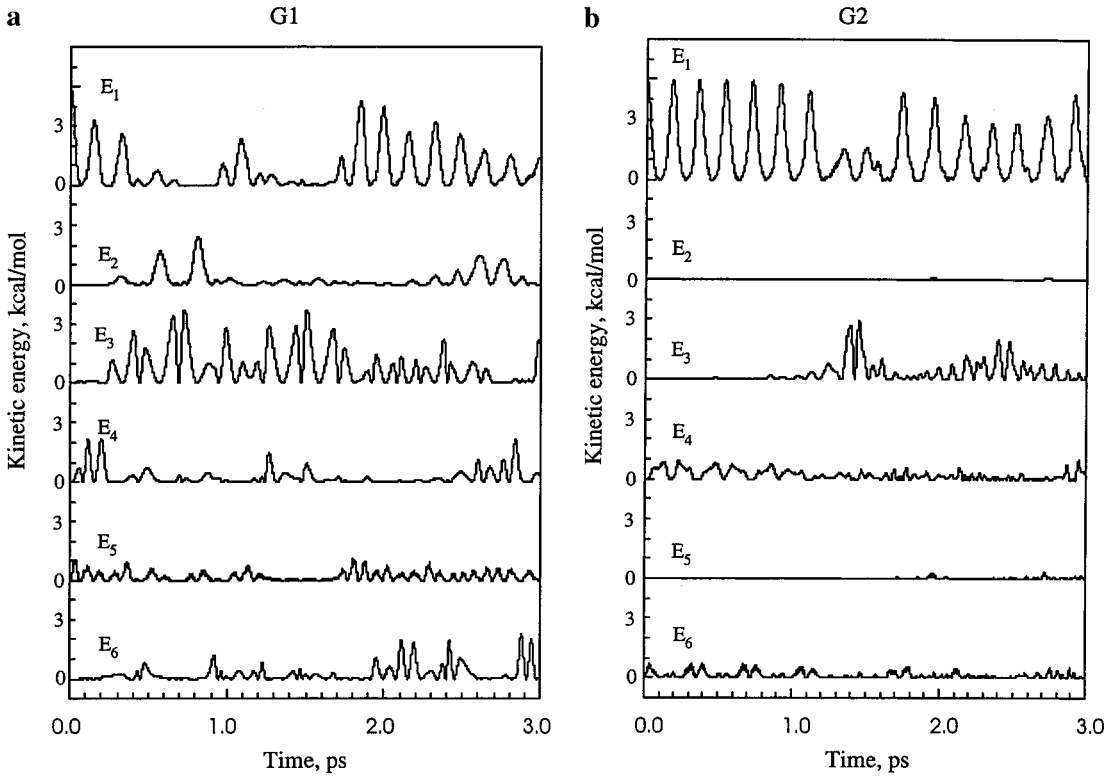


**Figure 5.** (a) Evolution of normal mode kinetic energy in structure G1. The initial kinetic energy of the first mode was set to 5 kcal/mol and that of all other modes was set to zero. Each successive curve is displaced upward by 5 kcal/mol for clarity. (b) Evolution of normal mode kinetic energy in structure G2. The initial kinetic energy of the first mode was set to 5 kcal/mol and that of all other modes was set to zero. Each successive curve is displaced upward by 5 kcal/mol for clarity.

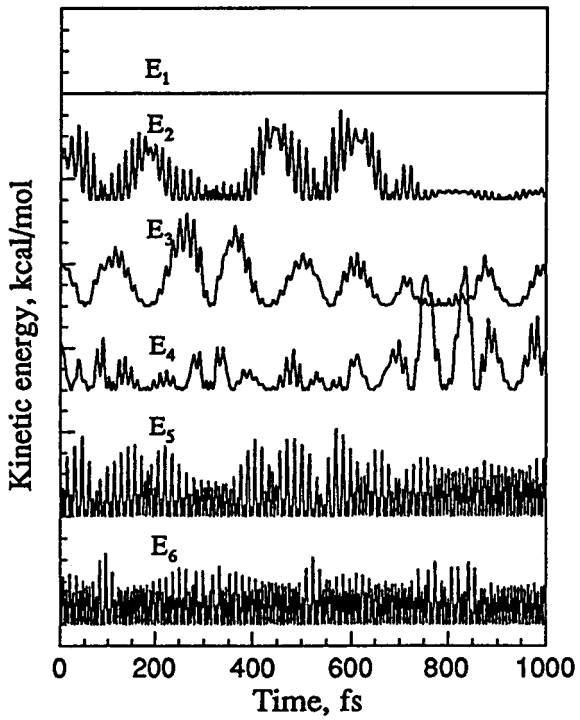


**Figure 6.** Evolution of normal mode kinetic energy in structure G1. The initial kinetic energy of the first mode was set to zero and that of all other modes was set to 1 kcal/mol. Each successive curve is displaced upward by 2.5 kcal/mol for clarity.

due to the complicated nature of mode coupling, and has not been previously clearly demonstrated.

The normal modes associated with antisymmetric bending are particularly interesting because they contribute heavily to the motion along the electron exchange reaction path (Table 2). The results of the previously discussed simulations indicate that antisymmetric bending modes of G1 and G2 are not coupled with the torsional mode, at least for the specific sets of initial conditions tested here (Figure 6 and Figure 5b). Additional MD simulations were carried out starting from the G1 and G2 ground-state geometries with initial kinetic energy of 5 kcal/mol in the corresponding second (bending) mode. Note that antisymmetric bending of G2 lowers molecular symmetry from $C_{2h}$ to $C_s$, so one would expect antisymmetric bending to mix with all other modes except the torsion. The results of these two simulations, displayed in Figure 7, support the symmetry analysis as the torsional modes remain nonexcited during 2 ps of simulation time. In other words, torsional rotation remains adiabatic, providing it does not have initial kinetic or potential energy.

In the next set of MD simulations we analyzed the energy transfer among stretching modes. Two simulations were carried out starting from the G1 and G2 geometries with initial kinetic energies of 5 kcal/mol placed into the corresponding stretching mode. The results of these simulations are displayed in Figure 8. No energy transfer from mode 5 to any other mode of the G1 complex was observed. In particular, modes 5 and 6 of this complex correspond to the stretching vibrations of CO and $CO^+$, respectively, and our results indicate that the vibrations of these two subunits are completely independent of each other on the simulation time scale. For the G2 complex, modes 5 and 6 correspond to the antisymmetric and symmetric stretching motion of all four atoms, respectively, and these two modes rapidly exchange energy (Figure 8b). Note that no energy transfer into the other four modes was observed in this simulation.

The observation of subsets of vibrational modes that do not exchange energy with other modes demonstrates the existence

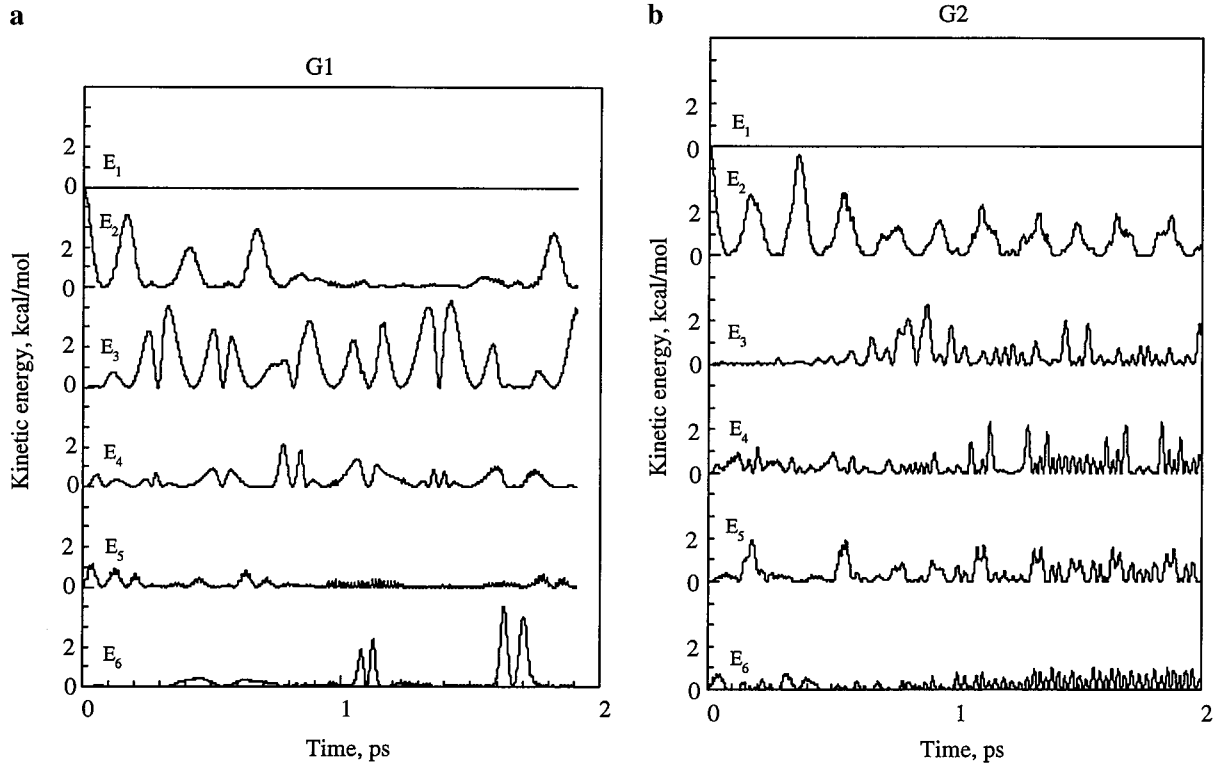


**Figure 7.** Evolution of normal mode kinetic energy in structure G1. The initial kinetic energy of the second mode was set to 5 kcal/mol and that of all other modes was set to zero. Each successive curve is displaced upward by 5 kcal/mol for clarity. (b) Evolution of normal mode kinetic energy in structure G2. The initial kinetic energy of the second mode was set to 5 kcal/mol and that of all other modes was set to zero. Each successive curve is displaced upward by 5 kcal/mol for clarity.

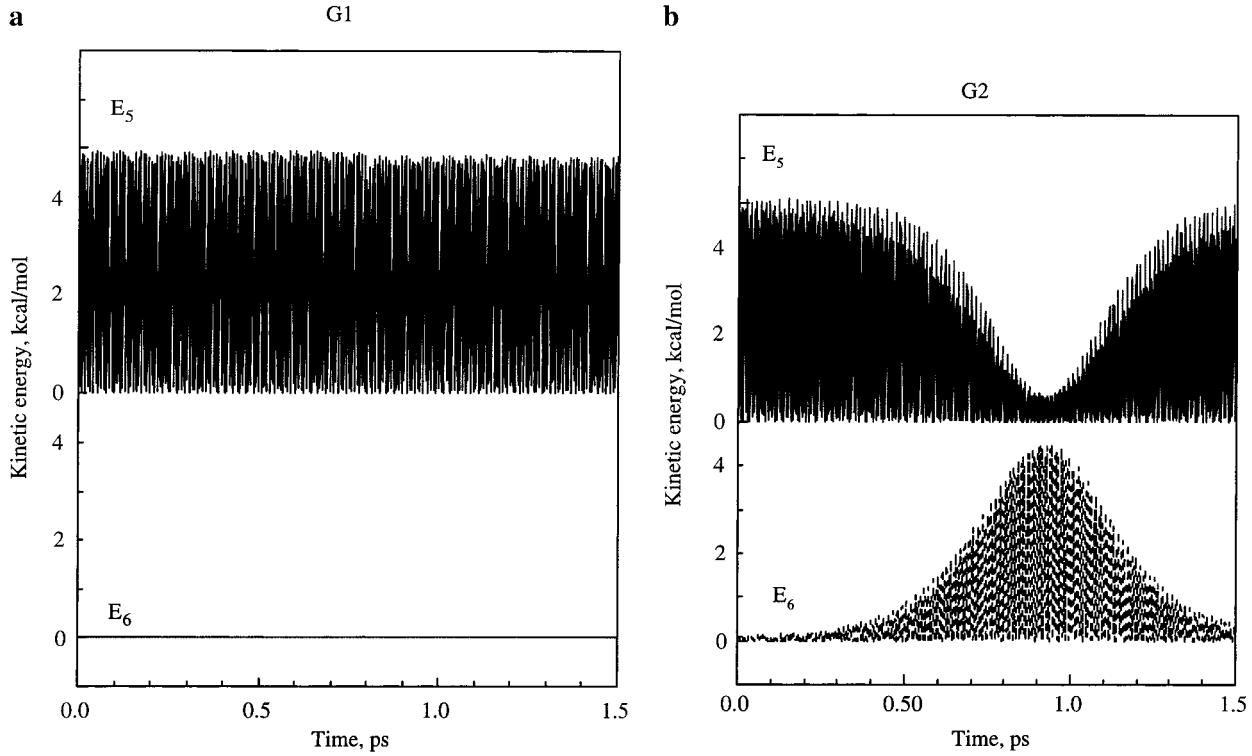


**Figure 8.** (a) Evolution of normal mode kinetic energy in structure G1. Short-time oscillations represent exchange between kinetic and potential energies *within the same mode*. In both simulations the initial kinetic energy of the fifth mode was set to 5 kcal/mol and that of all other modes was set to zero. Only modes 5 and 6 are displayed and the former is displaced upward by 5 kcal/mol for clarity. (b) Evolution of normal mode kinetic energy in structure G2. Short-time oscillations represent exchange between kinetic and potential energies *within the same mode*. In both simulations the initial kinetic energy of the fifth mode was set to 5 kcal/mol and that of all other modes was set to zero. Only modes 5 and 6 are displayed and the former is displaced upward by 5 kcal/mol for clarity.

of adiabatic normal mode manifolds for a specific set of initial conditions. The possible existence of adiabatic modes and mode manifolds was envisioned by Marcus[40] nearly 50 years ago, yet to our knowledge the present results are the first direct MD

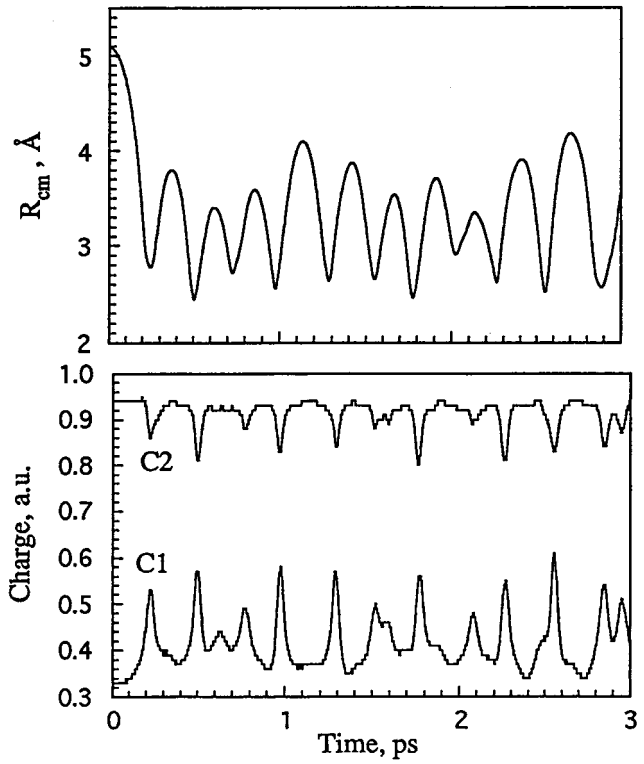


**Figure 9.** MO/MD simulation of the association of CO and $CO^+$. Top panel: Temporal evolution of the distance between centers of mass. Bottom panel: Temporal evolution of atomic charges.

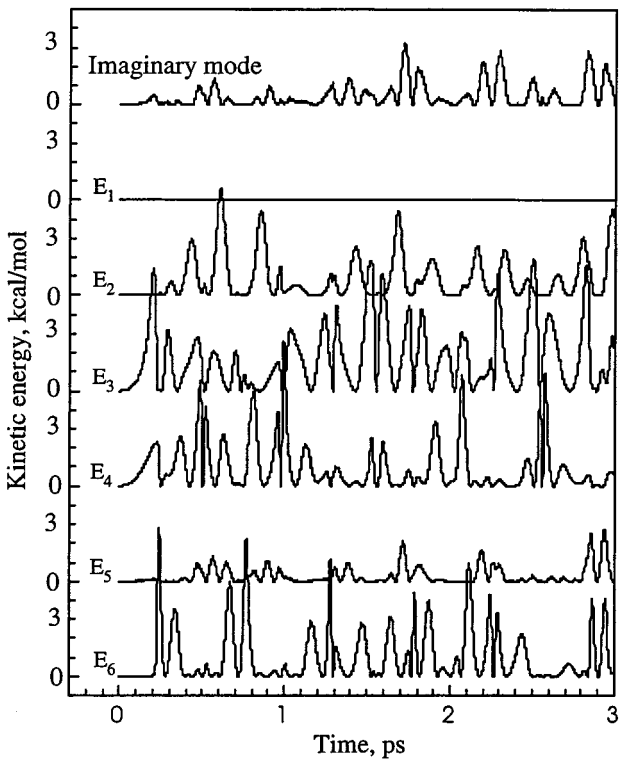


**Figure 10.** Temporal evolution of kinetic energy in the imaginary mode of TS1 and normal modes of G1 during MO/MD simulations of the association of CO and $CO^+$. Each successive curve is displace upward by 5 kcal/mol for clarity.

demonstration of these phenomena for vibrational modes which are typically considered as nonadiabatic. Although the simulation times reported here are very short, symmetry-forbidden energy exchange between vibrational modes will be rigorously maintained for as long as the system's symmetry is maintained. The presence of adiabatic modes and adiabatic mode manifolds for specific sets of initial conditions also implies that starting with the same energy but distributed differently among normal modes one would end up with different reaction rates, contrary to the prediction of statistical rate theories. This, however, does not necessarily imply that experimental thermally averaged rate constants will significantly differ from the theoretical, statistical result. Indeed, if systems with specific energy distributions (such as those discussed above) represent a small part of a microcanonical ensemble, their impact on the thermal rate constant would be negligible. For instance, the theoretical calculations for the association of $N_2$ and $N_2^+$ into the $(N_2)_2^+$ dimer (which we suggest is fairly similar to the reaction studied here) are in good agreement with experiment.[41]

To get further insight into the reaction dynamics we also modeled association of CO and $CO^+$ molecules starting from the point on the MEP with initial distance between molecules of 5 Å and zero initial kinetic energy. The potential energy at the starting point was 1.8 kcal/mol above the potential energy barrier or 10 kcal/mol above the G1 ground state. This simulation, moving from reactants to the transition state, can be viewed as a chemical activation process. The evolution of the distance and atomic charges during MD simulations is shown in Figure 9 and evolution of normal mode kinetic energies is displayed in Figure 10. One can see that the imaginary mode of TS1 and the CO stretching mode, which contributes the most into the imaginary mode (Table 2), are not acquiring energy directly from translational kinetic energy of two approaching molecules, but rather become excited due to energy transfer from other modes, after a short time delay. The reason for this is the reaction path curvature discussed above. Any set of initial conditions leads to some specific initial mode excitation, yet in the present case the modes contributing to the barrier crossing are not among those populated by chemical activation, and therefore, statistical rather than mode-specific behavior should be expected. From charge evolution one can deduce that no barrier crossing occurs during 3 ps of simulation. Both charge and intermolecular distances oscillate with frequency about 3.7 $ps^{-1}$, which is determined by the average width of the potential well at the given energy and corresponds to the effective frequency in the RRK expression:

$$k(E) = \nu\left(\frac{E - E_b}{E}\right)^{s-1}$$

where $E$ is the total energy, $E_b$ is the energy barrier, and $s$ is the number of active degrees of freedom. The evolution of the normal mode kinetic energy (Figure 10) shows that the torsional mode is adiabatic in this case and should be excluded from the active degrees of freedom. Substituting $s = 5$ into the above equation, we found $k(E) = 4 \times 10^{-3}$ $ps^{-1}$. Thus, at least 250 ps of simulation time is required to obtain a statistically meaningful estimate for rate constants and it is not surprising that barrier crossing was not observed in the present 3 ps time simulation.

To speed up barrier crossing we repeated MD simulations starting with the same initial geometry but with extra translational energies of 6.7 and 15 kcal/mol. The distance between the centers of mass of the CO and $CO^+$ fragments is displayed in Figure 11. One can see that no reaction occurs in both cases. The $CO\cdots CO^+$ complex dissociates before it can find the right transition state structure. Unfortunately, limited computer resources do not allow us to evaluate the rate constant from

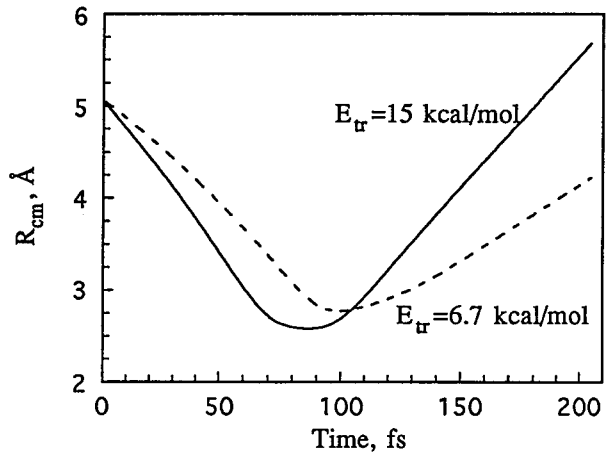


**Figure 11.** Temporal evolution of the distance between centers of mass of CO and $CO^+$ in MO/MD simulations started from the same geometry as in Figure 10, but with extra translational energy of 15 kcal/mol (solid line) and 6.7 kcal/mol (dashed line).

trajectory calculations and quantitative assessment must await future investigation.

## Conclusions

The potential energy surface, intramolecular energy transfer rates, and ET dynamics for electron self-exchange between CO and $CO^+$ were investigated by using MD methods with an ab initio, UHF/6-31G(d) potential. This work indicates some of the MO/MD method's limitations, and also demonstrates the method's potential for revealing intriguing, general implications for ET reactions.

First, it is found that the $CO + CO^+ \rightleftharpoons CO^+ + CO$ ET reaction proceeds through a triple-minimum potential well. The central, global minimum corresponds to the $(CO)_2^+$ dimer and two local minima correspond to weakly bound $CO\cdots CO^+$ capture complexes. We suggest that other ET reactions between polar diatomic molecules might proceed through similar triple-minimum potential wells. Charge transfer from CO to $CO^+$ is found to occur over a range of geometries different from intermediates or transition states, implying that calculating electron donor−acceptor coupling by using geometries of precursor complexes is inappropriate.

Second, Fourier transform methods were used to calculate vibrational and charge oscillation spectra from the MD simulations. Comparing the spectra and projecting the reaction coordinate on normal coordinates of the ET precursor (successor) complex and the intermediate implies that ET couples most strongly to *low*-frequency torsional and bending modes of $(CO)_2^+$. Thus, the common practice of assuming that ET couples exclusively to one or more high-frequency vibrations is unwarranted. Instead of calculating ET reorganization energies from vibrations of reactants and products, our work implies that vibrations of precursor and successor complexes should yield more accurate estimates of ET activation energies.

Next, energy transfer rates were computed from analysis of the time evolution of normal mode kinetic energies. The analysis shows that energy transfer processes are fast enough to ensure complete energy randomization on the reaction's time scale, yet the energy transfer is not globally rapid and is strongly affected by the choice of initial mode energies. We found that torsional rotation does not participate in energy exchange (e.g., it behaves adiabatically), as required by symmetry if its initial energy is set to zero. Similarly, stretching vibrations of CO and $CO^+$ in weakly bound complexes do not couple with other normal modes. It is interesting that, under certain conditions, symmetric and antisymmetric stretching modes of the $(CO)_2^+$ dimer form an adiabatic manifold, e.g., energy exchanges rapidly only between these two modes. Note that although low energy transfer rates have been reported for a number of systems, to our knowledge the existence of adiabatic vibrational modes and mode manifolds have not been previously demonstrated clearly. Our work thus implies that assumptions of energy randomization during ET—a foundation of transition state theories of ET[8]—should be tested, particularly for small, weakly coupled, and/or highly symmetrical structures. These are also the types of structures where manifold-specific reactions, similar to the mode-specific chemistry accomplished previously,[42] may ultimately prove possible.

**Acknowledgment.** This work was supported by the Office of Energy Research, Office of Basic Energy Sciences, U.S. Department of Energy under Contract No. DE-FG03-97ER14806. Supercomputer time at the NSF/National Center for Supercomputing Applications, provided through the NSF/National Resource Allocations Committee (Award No. MCA96N019), is gratefully acknowledged. Additional supercomputer time at the University of Oklahoma was made possible by support from the University of Oklahoma, IBM Corporation, and Silicon Graphics Inc.

## References and Notes

(1) Wheeler, R. A.; Skokov, S. *Abstracts of Papers*, 215th National Meeting of the American Chemical Society, April 2, 1998; American Chemical Society: Washington, DC, 1998; Vol. 215; pp PHYS 395.
(2) Barbara, P. F.; Meyer, T. J.; Ratner, M. A. *J. Phys. Chem.* **1996**, *100*, 13148−13168.
(3) Newton, M. D.; Sutin, N. *Annu. Rev. Phys. Chem.* **1984**, *35*, 437−480.
(4) Marcus, R. A.; Sutin, N. *Biochim. Biophys. Acta* **1985**, *811*, 265−322.
(5) Cannon, R. D. *Electron-Transfer Reactions*; Butterworth: London, 1980.
(6) Nesbitt, D. J.; Field, R. W. *J. Phys. Chem.* **1996**, *100*, 12735−12756.
(7) Zewail, A. *J. Phys. Chem.* **1996**, *100*, 12701−12724.
(8) Truhlar, D. G.; Garrett, B. C.; Klippensteinn, S. J. *J. Phys. Chem.* **1996**, *100*, 12771−12800.
(9) Marcus, R. A. *J. Chem. Phys.* **1965**, *43*, 679.
(10) Notable exceptions include: Markel, F.; Ferris, N. S.; Gould, I. R.; Myers, A. B. *J. Am. Chem. Soc.* **1992**, *114*, 6208−6219 and references therein.
(11) For example: Wyatt, R. E.; Iung, C.; Leforestier, C. *Acc. Chem. Res.* **1995**, *28*, 423−429 and references therein.
(12) Bianco, R.; Timoneda, J. J. I.; Hynes, J. T. *J. Phys. Chem.* **1994**, *98*, 12103 and references therein.
(13) Tuckerman, M. E.; Ungar, P. J.; von Rosenvinge, T.; Klein, M. L. *J. Phys. Chem.* **1996**, *100*, 12878−12887 and references therein.
(14) Warshel, A.; Parson, W. W. *Annu. Rev. Phys. Chem.* **1991**, *42*, 279−309 and references therein.
(15) Jortner, J.; Bixon, M. *J. Chem. Phys.* **1988**, *88*, 167.
(16) Newton, M. D. *Chem. Rev.* **1991**, *91*, 787−792.
(17) Methods for calculating donor−acceptor couplings at arbitrary geometries are now available: Cave, R. J.; Newton, M. D. *J. Chem. Phys.* **1997**, *106*, 9213−9226.
(18) Pellerite, M. J.; Brauman, J. I. *J. Am. Chem. Soc.* **1983**, *105*, 2672.
(19) Olmstead, W. N.; Brauman, J. I. *J. Am. Chem. Soc.* **1977**, *99*, 4219.
(20) Dodd, J. A.; Brauman, J. I. *J. Phys. Chem.* **1986**, *90*, 3559.
(21) Han, C.-C.; Wilbur, J. L.; Brauman, J. I. *J. Am. Chem. Soc.* **1992**, *114*, 887.
(22) Su, T.; Bowers, M. T. In *Gas Phase Ion Chemistry*; Bowers, M. T., Ed.; Academic: New York, 1979; Vol. 1; p 83.
(23) Rowe, B. R.; Dupeyrat, G.; Marquette, J. B.; Gaucherel, P. *J. Chem. Phys.* **1984**, *80*, 4915.
(24) Linn, S. H.; Ono, Y.; Ng, C. Y. *J. Chem. Phys.* **1981**, *74*, 3342−3347.
(25) Strobel, A.; Knoblauch, A. J.; Smith, A. M.; Niedner-Schatteburg, G.; Bondybey, V. *J. Phys. Chem.* **1995**, *99*, 872.
(26) Robinson, P. J.; Holbrook, K. A. *Unimolecular Reactions*; Stonebridge Press: Bristol, 1970.

(27) Forst, W. *Theory of Unimolecular Reactions*; Academic: New York, 1973.
(28) Linde, S. V.; Hase, W. L. *J. Phys. Chem.* **1990**, *94*, 6148.
(29) Pan, R.; Raff, L. M. *J. Phys. Chem.* **1996**, *100*, 8085.
(30) Carmer, C. S.; Weiner, B.; Frenklach, M. *J. Chem. Phys.* **1993**, *99*, 1353.
(31) Skokov, S.; Carmer, C. S.; Weiner, B.; Frenklach, M. *Phys. Rev. B* **1994**, *49*, 5662−5671.
(32) Schmidt, M. W.; Baldridge, K. K.; Boatz, J. A.; Jensen, J. H.; Koleski, S.; Gordon, M. S.; Nguyen, K. A.; Windus, T. L.; Elbert, S. T. *QCPE Bull.* **1990**, *10*, 52.
(33) Berendsen, H. J. C.; Postma, J. P. M.; Gunsteren, W. F.; DiNola, A.; Haak, J. R. *J. Chem. Phys.* **1984**, *81*, 3684.
(34) Mulliken, R. S. *J. Chem. Phys.* **1955**, *23*, 1833−1840.
(35) Futrele, R. P.; McGinty, D. J. *Chem. Phys. Lett.* **1971**, *12*, 285−287.
(36) Scott, A. P.; Radom, L. *J. Phys. Chem.* **1996**, *100*, 16502−16513.
(37) Raff, L. M. *J. Chem. Phys.* **1988**, *89*, 5680−5691.
(38) Herzberg, G. *Molecular Spectra and Molecular Structure*; Robert E. Krieger Publishing: Malabar, Florida, 1989; Vol. 1; p 521.
(39) Frisch, M. J.; Trucks, G. W.; Schlegel, H. B.; P. M. W. Gill; Johnson, B. G.; Robb, M. A.; Cheeseman, J. R.; Keith, T.; Petersson, G. A.; Montgomery, J. A.; Raghavachari, K.; Al-Laham, M. A.; Zakrzewski, V. G.; Ortiz, J. V.; Foresman, J. B.; Cioslowski, J.; Stefanov, B. B.; Nanayakkara, A.; Challacombe, M.; Peng, C. Y.; Ayala, P. Y.; Chen, W.; Wong, M. W.; Andres, J. L.; Replogle, E. S.; Gomperts, R.; Martin, R. L.; Fox, D. J.; Binkley, J. S.; Defrees, D. J.; Baker, J.; Stewart, J. P.; Head-Gordon, M.; Gonzalez, C.; Pople, J. A. *GAUSSIAN94*; D.1 ed.; Gaussian, Inc.: Pittsburgh, PA, 1995.
(40) Marcus, R. A. *J. Chem. Phys.* **1952**, *20*, 359−364.
(41) Herst, E. *J. Chem. Phys.* **1980**, *72*, 5284.
(42) Crim, F. F. *J. Phys. Chem.* **1996**, *100*, 12725−12734.